Remote sensing of aerosol optical depth over central Europe from MSG-SEVIRI data and accuracy assessment with ground-based AERONET measurements

C. Popp,[1] A. Hauser,[2] N. Foppa,[3] and S. Wunderle[1]

Received 15 January 2007; revised 26 May 2007; accepted 4 June 2007; published 9 November 2007.

[1] In this study, the remote sensing of aerosol optical depth (τ_a) from the geostationary Meteosat Second Generation (MSG) Spinning Enhanced Visible and Infrared Imager (SEVIRI) is demonstrated. The proposed method is based on the analysis of a time series of SEVIRI's 0.6 μm channel images. Top-of-atmosphere reflectance is precorrected for the effect of atmospheric gases and a background aerosol amount. Subsequently, surface reflectance for each pixel is estimated by determining its lowest precorrected reflectance within the observed time period for each satellite observation time of the day. The resulting diurnal surface reflectance curve in combination with the radiative transfer code SMAC are finally used to derive τ_a. This approach is applied to SEVIRI subscenes of central Europe (40.8–51.3°N, 0.3°W–19.9°E) from August 2004, daily acquired between 0612 and 1712 UTC in intervals of 15 min. SEVIRI τ_a are related to Aerosol Robotic Network (AERONET) Sun photometer measurements from nine sites. About 3200 instantaneous SEVIRI and Sun photometer τ_a are compared. An overall correlation of 0.9 and a root mean square error of 0.08 are obtained. Further, the spatial distribution of SEVIRI τ_a maps for August 2004 represent expectable features like higher concentrations in industrialized regions or lower loading in higher altitudes. It is concluded that the described method is able to provide an estimate of τ_a from MSG-SEVIRI data. Such aerosol maps of high temporal frequency could be of interest to atmospheric related sciences, e.g., to track aerosol particle transport.

Citation: Popp, C., A. Hauser, N. Foppa, and S. Wunderle (2007), Remote sensing of aerosol optical depth over central Europe from MSG-SEVIRI data and accuracy assessment with ground-based AERONET measurements, *J. Geophys. Res.*, *112*, D24S11, doi:10.1029/2007JD008423.

1. Introduction

[2] Since atmospheric aerosols highly vary in their chemical and physical properties as well as in their spatiotemporal distribution, the description and quantification of their direct and indirect effects on the global radiation budget still is a challenging and complex task in today's atmospheric and climate related science. The third assessment report of the Intergovernmental Panel on Climate Change (IPCC) in 2001 outlined five different types of investigations needed to gain further insights on the role and impacts of aerosols, among them measurements from spaceborne instruments [*Intergovernmental Panel on Climate Change*, 2001]. Particularly the ability of remote sensing to provide spatially homogeneous data offers a unique occasion to complement the spacing from ground-based measurements. Attempts toward a global aerosol climatology based on spaceborne measurements have been performed using the Total Ozone Mapping Spectrometer (TOMS [*Torres et al.*, 2002]) or the Advanced Very High Resolution Radiometer (AVHRR [*Geogdzhayev et al.*, 2005]) whose records date back more than 20 a. During the last decade, advanced sensors and techniques like, e.g., the Moderate Resolution Imaging Spectrometer (MODIS [*Kaufman et al.*, 1997a; *Tanré et al.*, 1997]), the Multiangle Imaging Spectroradiometer (MISR [*Martonchik et al.*, 1998]), or the Directionality of the Earth's Reflectances sensor (POLDER [*Deuzé et al.*, 2001]) further enhanced aerosol characterization from space over land and ocean. However, the nature of polar orbiting instruments does not allow to account for the diurnal variations of atmospheric aerosol parameters. Up-to-date geostationary instruments like the Spinning Enhanced Visible and Infrared Imager (SEVIRI) on board the current and future satellites of the Meteosat Second Generation (MSG) offer considerable prospects to enhance the frequency of aerosol mapping. Their high temporal resolution supplementary increases the probability of finding cloud-free observations at individual image locations.

[3] Saharan dust outbreaks over the Atlantic Ocean [*Jankowiak and Tanré*, 1992] and over the Mediterranean

[1]Department of Geography, University of Bern, Bern, Switzerland.
[2]EADS Astrium GmbH, Immenstaad, Germany.
[3]Swiss Federal Office of Meteorology, Zurich, Switzerland.

0148-0227/07/2007JD008423

[*Moulin et al.*, 1997] have been studied on the basis of data from the Meteosat Visible and InfraRed Imager (MVIRI) of the Meteosat First Generation platforms. The nonsphericity of such mineral dust particles has been considered in the work of *Masuda et al.* [2002] with data from the Japanese Geostationary Meteorological Satellite (GMS-5). Ångström exponent (α) and aerosol optical depth (τ_a) have been retrieved from the same instrument over the western Pacific ocean in the study of *Wang et al.* [2003]. Smoke aerosol optical thickness based on data from the Geostationary Observational Environmental Satellite (GOES) has been derived by *Zhang et al.* [2001] and *Knapp et al.* [2002] who extended the aerosol characterization from geostationary sensors to land surfaces. *Knapp* [2002] quantified the aerosol signal over the North American continent in GOES 8 imagery leading to a further broadening of geostationary aerosol retrieval with regard to different land cover types and aerosol regimes [*Knapp et al.*, 2005].

[4] SEVIRI's enhanced spectral, spatial, and temporal characteristics in comparison to its predecessor MVIRI on board Meteosat 1–7 offers new potentials in using these data to characterize and to track atmospheric aerosols over Africa and Europe. For instance, MVIRI's only band in the visible and near infrared (VIS, 0.45 to 1.0 μm) is replaced by three narrower bands at 0.6 μm, 0.8 μm, and 1.6 μm. The NOAA/National Environmental Satellite, Data, and Information Service (NESDIS) third generation aerosol retrieval algorithm [*Ignatov and Stowe*, 2002a] for the AVHRR has been adapted to SEVIRI data for the retrieval of mineral τ_a and aerosol size information over ocean [*Brindley and Ignatov*, 2006]. A similar purpose has been pursued in the work of *Thieuleux et al.* [2005]. Another technique quantifies Saharan dust outbreaks using SEVIRI's thermal infrared bands with the aim for resolving the impact of dust misidentification as clouds in the Geostationary Earth Radiation Budget (GERB, also on board the MSG platforms) derived shortwave and longwave fluxes [*Brindley and Russell*, 2006]. So far, these approaches are restricted to ocean surfaces and aerosol particles originating from a desert environment.

[5] The objective of this study is to apply a single-channel, multitemporal method for the remote sensing of τ_a from SEVIRI imagery over various surface types in order to demonstrate its potentials and limitations for providing aerosol information. The outline of the methodology points to a possible operational retrieval of τ_a from the European meteorological geostationary satellites of the second generation. The proposed method does not intrinsically require any a priori information. In addition, the anisotropic characteristics of a majority of natural surfaces is considered in the estimation of surface reflectance by taking advantage of the fixed viewing angles of geostationary sensors. Aerosol maps of temporal high frequency can be of great interest to atmospheric related science, e.g., to study the interaction between aerosols and clouds or to observe the relation between aerosols and synoptic weather systems.

2. Data

2.1. SEVIRI Data

[6] SEVIRI measures reflected and emitted radiance in 11 spectral channels located between 0.6 μm and 14 μm and in one broadband high-resolution visible (HRV, 0.4–1.1 μm) channel. The solar channels dedicated to derive atmospheric aerosol parameters are centered at 0.6 μm (0.56–0.71 μm), 0.8 μm (0.74–0.88 μm), and 1.6 μm (1.50–1.78 μm), respectively and have a nominal spatial resolution of 3 km at the subsatellite point ($\sim$5 km for central Europe) as well as a temporal sampling rate of 15 min. SEVIRI represents a significant technical advancement to MVIRI on board Meteosat-1 to 7 with its three spectral channels, a spatial resolution of 5 km at the subsatellite point, and a repetition rate of 30 min. Started in August 2002 with the launch of MSG-1 (renamed to Meteosat-8 once in orbit) and operationally providing data since January 2004, the MSG program ensures the continuity of the European geostationary meteorological satellite service until around 2018 [*Schmetz et al.*, 2002].

[7] Meteosat-8 SEVIRI Level 1.5 geolocated and calibrated top-of-atmosphere reflectance (ρ_{TOA}) data acquired daily between 0612 and 1712 UTC are used herein to perform the τ_a retrieval. SEVIRI's solar channels are calibrated with a vicarious approach and the calibration errors are reported to be lower than 5% [*Govaerts and Clerici*, 2004]. Also, multitemporal image coregistration is supposed to be less then 1.2 km (or 0.4 pixel) at the subsatellite point [*Hanson and Mueller*, 2004]. The month of August is chosen for a first implementation since the atmospheric aerosol concentration is expected to be higher, daytime is longer, and the probability of cloud and snow contamination of the data set smaller in comparison to other seasons. The study area is limited to central Europe (40.8–51.3°N, 0.3°W–19.9°E, see Figure 1).

[8] Adequate cloud screening is an essential preprocessing step in τ_a retrieval since undetected cloud pixels lead to a serious overestimation of τ_a, probably even outnumbering the performance of the retrieval algorithm itself [*Ignatov and Stowe*, 2002b]. A directly opposed effect is expected to be introduced by cloud shadows. Cloudy pixels are masked out in the imagery data set with a multispectral threshold approach according to *Derrien and Le Gléau* [2005]. As a side effect, the same algorithm also separates snow covered pixels. A procedure originally developed to detect and remove cloud shadows from AVHRR data [*Simpson and Stitt*, 1998] is subsequently conducted. This method is based on the cloud mask and 0.8 μm channel imagery. A series of tests are applied on the standard deviation of ρ_{TOA} in variable sized boxes around the cloud edge to identify cloud shadow pixels over land taking advantage of the larger contrast of clear and cloud shadowed pixels in the 0.8 μm channel.

2.2. AERONET Data

[9] The Aerosol Robotic Network (AERONET) is a global aerosol monitoring network of ground based Sun photometer (SP) measurements. Cloud-screened and quality-assured level 2.0 data [*Smirnov et al.*, 2000] is used to validate retrieved τ_a and to evaluate the estimation of surface reflectance. The accuracy of level 2.0 data is expected to be ±0.02 [*Holben et al.*, 1998]. Additionally, the AERONET measurements are log-linearly interpolated [*Ångström*, 1961] to the reference wavelength at 0.55 μm used hereafter. Table 1 summarizes the nine AERONET sites from which level 2.0 data is available for the described

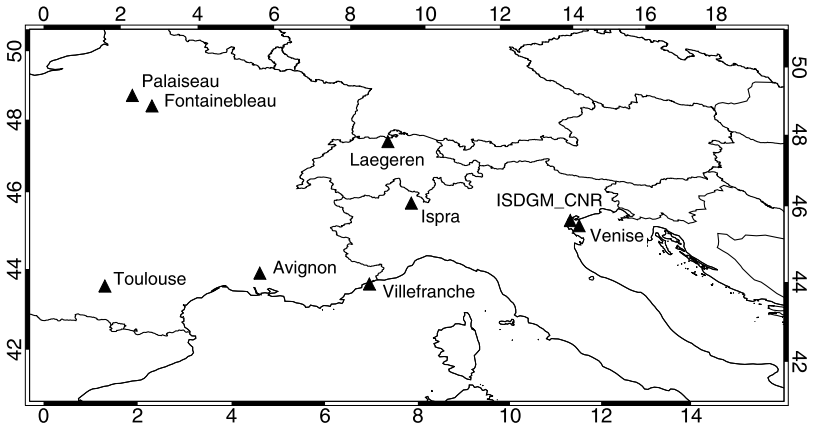

Figure 1. Investigation area and the locations of the AERONET sites.

time period and Figure 1 shows their locations in central Europe. The specified sites reflect divers surface cover types which are roughly outlined in the last column of Table 1 based on the site information given on the AERONET Web site (http://aeronet.gsfc.nasa.gov).

2.3. MODIS Data

[10] In addition to the validation using SP measurements, the SEVIRI results are also compared to the daily MODIS Collection 005 products MOD04L2 (TERRA) and MYD04L2 (AQUA) which allows a better assessment of the retrieval performance with regard to its geographical distribution. The MODIS aerosol parameters from the investigated time period are therefore reprojected and resampled to the SEVIRI grid. MODIS derived τ_a are expected to be within $0.05 \pm 0.2\tau_a$ over land and $0.03 \pm 0.05\tau_a$ over ocean [*Chu et al.*, 2002; *Remer et al.*, 2005]. The combined land and ocean product or scientific data set "Optical_Depth_Land_Ocean" is used in this study. The high temporal resolution of SEVIRI allows a close matchup to MODIS overpasses such that the differences of coincident MODIS-SEVIRI comparisons do not exceed 7.5 min.

2.4. Meteorological Data

[11] Meteorological auxiliary data from the Swiss Federal Office of Meteorology and Climatology's Alpine Model (aLMo) and from the National Center for Environmental Prediction (NCEP) are used to obtain additional information about the state of the atmosphere during the time of image acquisition and to avoid the assumption of a standard atmosphere. Total column ozone data on a $1° \times 1°$ grid (NCEP) are available for each day at 0600, 1200, and 1800 UTC, vertically integrated water vapor and sea level pressure with a horizontal grid size of 7 km (aLMo) are available for each day at 1200 UTC.

3. Aerosol Optical Depth Retrieval

[12] In general, the methodologies to retrieve atmospheric aerosol information predominantly depend on the sensor's spectral, spatial, and temporal properties as well as on the area investigated, in particular with regard to its surface brightness. An overview of different techniques, sensors, and their applicability is given by *King et al.* [1999] and more recently by *Yu et al.* [2006]. Initially, a few considerations should be made on the basis of SEVIRI's characteristics and the aim to derive τ_a in midlatitude regions like the area of interest of this study. The crucial step to determine aerosol information from remotely sensed data is the decomposition of ρ_{TOA} into its surface (ρ_{SURF}) and atmospheric (ρ_{ATM}) contribution. As outlined in many studies [e.g., *Kaufman et al.*, 1997b; *King et al.*, 1999], the maximum sensitivity to the aerosol signal is at least in the spectral domain of SEVIRI's solar channels consequently given over low-reflecting surfaces. Hence the start in many τ_a retrieval algorithms is an appropriate classification of such surface targets and the subsequent estimation of their reflectivity. This step is frequently addressed by finding dark dense vegetation pixels (DDV) in the image data [*Kaufman and Sendra*, 1988; *Kaufman et al.*, 1997a]. However, these approaches are often limited by the sparse distribution of DDV pixels in many regions, for instance, *Borde et al.*

Table 1. Summary of the AERONET Sites Used in This Study and Their Geographical Locations[a]

Site Name	Latitude	Longitude	Altitude, m asl	Characteristic
Avignon	43°55′N	4°52′E	32	agriculture, suburbia
Fontainebleau	48°24′N	2°40′E	85	forest, residential area
ISDGM_CNR	45°26′N	12°19′E	20	urban, water
Ispra	45°48′N	8°37′E	235	forest, water, agriculture
Laegeren	47°28′N	8°21′E	735	forest, agriculture
Palaiseau	48°42′N	2°12′E	156	residential area, agriculture
Toulouse	43°34′N	1°22′E	150	suburbia
Venise	45°18′N	12°30′E	10	water, off shore
Villefranche	43°41′N	7°19′E	130	peninsula, water

[a]Also given are the surface characteristics at the single sites. The most dominant characteristic appears first.

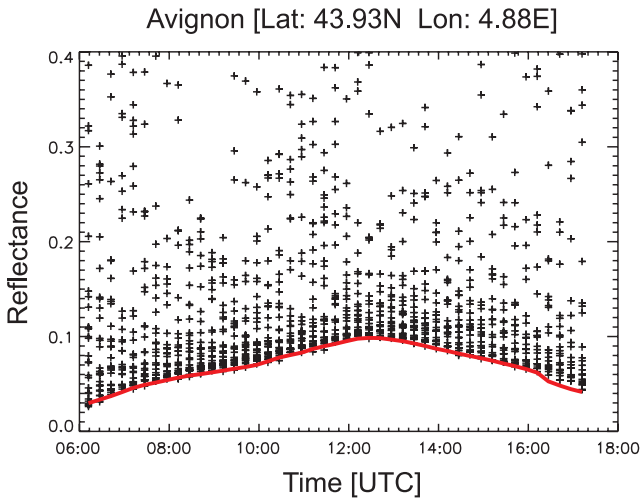

Figure 2. Retrieving estimated surface reflectance as a function of the image acquisition time (ρ_{SURF_EST}, red curve) exemplified for the pixel assigned to the AERONET site of Avignon. The plus signs illustrate the entire precorrected and cloud-screened data set with the exception of values not passing the cloud shadow threshold of 0.005.

[2003] found less than 1% DDV pixels in a scene from the Modular Optoelectronic Scanner (MOS) over southwest France. Further, SEVIRI does not include a 2.1 μm channel to estimate ρ_{SURF} at 0.6 μm as performed by the MODIS operational algorithm for the remote sensing of aerosols over land [*Kaufman et al.*, 1997a; *Remer et al.*, 2005]. *Liang et al.* [2006] recently used temporal signatures to extend the MODIS algorithm to a wider range of surface types. The concept of multitemporal image analysis in order to derive τ_a over land has been adopted to polar-orbiting sensors such as the Landsat Thematic Mapper [*Tanré et al.*, 1988] or the AVHRR [*Holben et al.*, 1992; *Knapp and Stowe*, 2002; *Hauser et al.*, 2005a] as well as to geostationary sensors [*Zhang et al.*, 2001; *Knapp et al.*, 2005]. The high scanning frequency of the latter favors the application of a multitemporal approach also for SEVIRI.

3.1. Surface Reflectance Estimate and Inversion of τ_a

[13] For a first attempt to derive τ_a from SEVIRI, the 0.6 μm channel is chosen since in the absence of dust particles the aerosol scattering usually decreases with increasing wavelength. Supplementary, the reflectance of a majority of natural land surfaces is lowest in the 0.6 μm channel in contrary to the channels at longer wavelength (0.8 μm, 1.6 μm). The bright surfaces (especially vegetation) in these two channels significantly reduce the sensitivity to an aerosol signal hindering a meaningful retrieval of τ_a. While the observation angles of geostationary sensors remain invariable, ρ_{SURF} (and therewith ρ_{TOA} measurements) depends on varying illumination angles and changes during the course of the day. The dependence of ρ_{SURF} on the observation geometry is commonly described by the bidirectional distribution function (BRDF) which shall be approximated in a first step to retrieve τ_a. For this purpose, it is assumed that the surface characteristic at each image location does not change during the observation period of 31 d and that there is at least one observation under "aerosol-free" condition for each pixel and each acquisition time. The 31 d are chosen because they are in the range of what is reported in the literature, e.g., 30 d [*Zhang et al.*, 2001], 7 to 28 d [*Knapp et al.*, 2005], 45 d [*Hauser et al.*, 2005a], and 3 months [*Liang et al.*, 2006]. It can also be expected that surfaces are more stable during summer months than in spring or fall when vegetation changes. Nevertheless, this stability criterion is evaluated latter.

[14] Since AERONET (or the distribution of its sites, Figure 1) does not provide spatial homogeneous information about aerosol type and minimum atmospheric aerosol amount which could be related to the entire study area, these parameters have to be a priori assumed. The continental aerosol type as incorporated in the 6S radiative transfer code [*Vermote et al.*, 1997a] is the model of choice based on the geographical study area. This model represents a mixture of the three basic components dust-like (0.70 volume percentage), water soluble (0.29), and soot (0.01) (defined by *World Meteorological Organization* [1983]) and the single scattering albedo (ω_0) at 0.55 μm is 0.89. The "aerosol-free" observation is attributed to an atmosphere with an assumed background aerosol optical depth (τ_{a_bck}) of 0.05 according to previous studies [*Knapp et al.*, 2002; *Hauser et al.*, 2005a]. These assumptions are elaborated in detail in sections 4.2.2 and 4.2.3.

[15] The data set then is prepared by precorrecting ρ_{TOA} for gaseous absorption, Rayleigh scattering, and the background aerosol extinction. The 6S based Simplified Method for Atmospheric Correction (SMAC [*Rahman and Dedieu*, 1994]) radiative transfer code is used for radiative transfer calculations because of its ability to handle larger data volumes within reasonable time and with sufficient accuracy. The BRDF for each pixel subsequently is approximated by plotting the precorrected reflectances as a function of the diurnal observation time and extracting the lowest value per observation time (Figure 2). Undetected cloud shadow pixels are addressed by rejecting land pixels with ρ_{SURF} lower than 0.005. This threshold is chosen because it separates the two modes of the histogram found for ρ_{SURF}. A boxcar average with a width of 5 finally is applied on the resulting background curve to compensate for minor inaccuracies which could be introduced by, e.g., undetected cloud shadows, overcorrection or undercorrection, or inaccurate meteorological data. The determined ρ_{SURF} curve (herein after referred to as ρ_{SURF_EST} to differentiate between "real" and estimated surface reflectance) in Figure 2 demonstrates the ability of this method to approximate the anisotropic reflectance characteristics of most natural surfaces. Considering the exemplary pixel at the Avignon site, ρ_{SURF_EST} decreases with larger Sun zenith angles in the morning and later afternoon.

[16] Reflectance estimation for water is performed similar to the one for land surfaces. Sun-glint affected regions over water are rejected from further processing by applying a 30° threshold on the glint cone angle (analog to *Brindley and Ignatov* [2006]) and the lower reflectance threshold of 0.005 over land is not applied on water pixels. The minimum glint angle found in the data set is 23° (1 August) which increases to 32° for 31 August. For physical reasons, overcorrected water pixels with ρ_{SURF_EST} lower than zero are excluded.

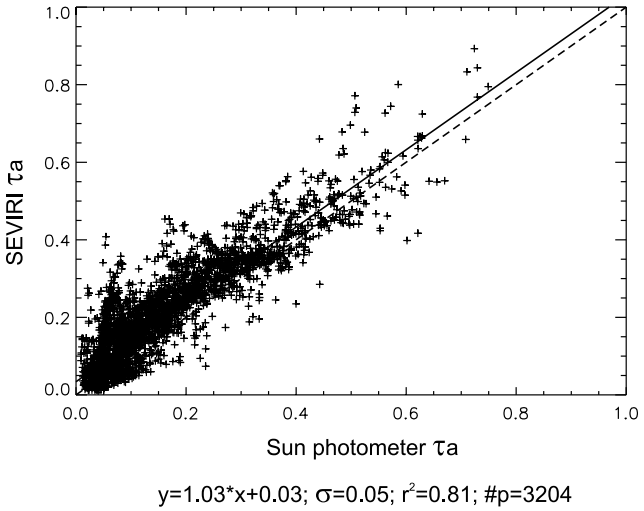

Figure 3. Scatterplot for the collective SEVIRI-AERONET matchups with linear regression line (solid) and bisecting line (dashed).

[17] Once ρ_{SURF_EST} is determined for each pixel, τ_a is computed for every cloud and cloud shadow free pixel in the test data set reusing the above mentioned meteorological data set and the assumed continental aerosol model. The computational efficiency of SMAC enables the application of an iterative inversion procedure in order to compute τ_a avoiding the calculation and implementation of look-up tables.

3.2. Spatial Consistency

[18] Potential errors in the resulting τ_a might be due to different sources which are discussed in detail in sections 4.2.1 to 4.2.4. Residual cloud contamination is despite the incorporated cloud and cloud shadow mask still very likely to occur thus introducing large deviations of τ_a. Especially the effect of subpixel clouds is difficult to account for but can become of great importance with regard to SEVIRI's spatial resolution. Also, it can be expected that the retrieval error increases with increasing surface reflectance due to the decreased sensitivity of the sensor to an aerosol signal. Taking advantage of the spatial dependency of adjacent τ_a, the primary estimations of τ_a are filtered in the spatial scale to reduce the impact of the above mentioned factors. Spatial consistency tests are frequently used to reduce the impact of, e.g., clouds or other contamination in remotely sensed data. For instance, the operational MODIS aerosol algorithm (over land) uses exclusively the 20 to 50 percentile of the measured radiance inside a 10×10 km^2 box [*Remer et al.*, 2005] as well as a threshold on the standard deviation from 3×3 pixel boxes to exclude clouds (over oceans [*Martins et al.*, 2002]). Regarding SEVIRI's spatial resolution of approximately 5 km for the central European region, a box size of 5×5 pixels (25×25 km^2) is chosen herein to obtain a sufficient statistical sample. The consistency tests are performed on τ_a as the aerosol load in the chosen region can be expected to be more or less stable in contrary to the surface reflectance of the individual pixels which might vary substantially. Choosing a larger window size increases the probability of spatially inhomogeneous aerosol characteristics. If nine or more valid retrievals are found inside the window, the average τ_a of its 20 to 50 percentile is assigned to its central pixel and the standard deviation of this percentile is recorded. It is found that only 6% of the boxes have a local standard deviation higher than 0.05 and less than 4% higher than 0.06. Because of the marginal difference, the more conservative threshold of 0.05 is chosen.

4. Results and Validation

[19] The analysis and validation of SEVIRI retrieved τ_a is based on comparisons to AERONET SP measurements. First, SEVIRI estimated and SP τ_a have to be collocated in the spatial and temporal domain. All available SP measurements within ±15 min to the SEVIRI observation time are averaged and then related to the SEVIRI estimate. Note that each SEVIRI value already represent a 5×5 pixel box around the AERONET site (section 3.2). The time interval of 30 min and the 25×25 km^2 box allow to account for both, the spatial variability of SEVIRI τ_a and the temporal variability of SP τ_a.

[20] Regression analysis of the retrieval results as a function of SP measurements is commonly used to address the performance of aerosol information from remote sensing data [*Ignatov and Stowe*, 2000; *Zhao et al.*, 2002, 2004]. Following this approach, an intercept different to zero points to a bias of low τ_a which is probably caused by calibration inaccuracies or an underestimation or overestimation of ρ_{SURF_EST}. A slope of the regression line not equal to unity is assigned to inappropriate assumptions of the aerosol model (i.e., ω_0). The standard error (σ) points to random errors like ρ_{SURF} variability or subpixel cloud contamination. In addition, the correlation coefficient (R) is used as an indicator of SEVIRI's capability to detect an aerosol signal over specific surfaces. The ability to sense an aerosol signal however, does not per se enable an accurate τ_a retrieval.

[21] In this section, simultaneous as well as daily averaged SEVIRI and SP τ_a are compared (section 4.1) in order to achieve the potential and limitation of MSG-SEVIRI for the remote sensing of aerosols over land and water surfaces. The accuracy of ρ_{SURF_EST} is evaluated in section 4.2.1 because it is supposed that ρ_{SURF_EST} is the most critical parameter in the retrieval. Further, a general reflection of additional sources of errors is given (sections 4.2.1 to 4.2.4) and the capabilities and limitations are subsequently underlined by selected aerosol maps and a comparison to the operational MODIS aerosol product (section 4.3.2).

4.1. Validation Using AERONET

[22] Figure 3 illustrates the SEVIRI retrieved τ_a as a function of the SP measurements and Table 2 summarizes the corresponding statistical parameters from the linear regression analysis of all SEVIRI-AERONET matchups for each site separately. About 3200 valid matchups are retrieved for all AERONET sites which is about 26% of all possible SEVIRI observations. The number of matchups varies from site to site and substantially depends on the cloud coverage at the individual locations and/or on the availability of AERONET observations. The sites in the southern part, namely Venise, Villefranche, ISDGM-CNR, and Avignon generally permit more valid retrievals. The third column of Table 2 shows the mean values of the

Table 2. Summary of the Statistical Parameters From the Linear Regression Analysis of SEVIRI and AERONET Sun Photometer Matchups

AERONET Site	Number of Matchups	% of Total	$\overline{\rho_{SURF\_EST}}$	Intercept	Slope	σ	Bias	R	RMSE
All sites	3204	26%	0.047	0.03	1.03	0.05	0.06	0.90	0.08
Avignon	511	37%	0.070	0.05	1.16	0.06	0.09	0.82	0.11
Fontainebleau	84	6%	0.067	0.01	1.07	0.05	0.06	0.89	0.08
ISDGM_CNR	526	38%	0.032	0.07	0.93	0.04	0.06	0.93	0.07
Ispra	365	26%	0.026	0.04	0.98	0.04	0.05	0.97	0.06
Laegeren	237	17%	0.049	0.04	0.98	0.04	0.05	0.85	0.07
Palaiseau	106	8%	0.088	−0.02	1.38	0.05	0.07	0.76	0.08
Toulouse	268	19%	0.085	0.04	1.16	0.07	0.08	0.72	0.11
Venise	649	47%	0.000	0.02	1.08	0.03	0.04	0.96	0.05
Villefranche	458	33%	0.008	−0.02	1.23	0.03	0.03	0.95	0.05

ρ_{SURF_EST} curves from the 5 × 5 pixel boxes ($\overline{\rho_{SURF\_EST}}$) around each site as an indicator of surface brightness.

[23] The overall R of 0.90 references to a generally good agreement between SEVIRI retrievals and SP measurements. The slope is within 3% to unity supporting the continental aerosol type to adequately mirror the average aerosol type of the investigation area. The overall intercept of 0.03 denotes a common underestimation of ρ_{SURF_EST} which is underlined by the systematic error or bias of 0.06. A majority of the points lie above the bisecting line documenting the generally resulting overestimation of τ_a. Further, the standard error of 0.05 reveals some scattering introduced by random errors and a total root mean square error (RMSE) of 0.08 is found. It is also noteworthy that 75% of all matchups and 71% if the matchups from the offshore site of Venise are excluded are within the MODIS uncertainty over land of $0.05 \pm 0.20\tau_a$ [*Remer et al.*, 2005].

[24] The statistical parameters computed for the single AERONET sites provide some further insight in the retrieval performance. Apart from Villefranche and Palaiseau, all stations show positive intercepts which range from 0.02 to 0.07. Villefranche and Venise are special cases since Venise lies approximately 16 km offshore in the Adriatic Sea. The AERONET site of Villefranche in fact is located on land, but on a small peninsula within a distance of only a few hundred meters to the Mediterranean Sea. The relatively low $\overline{\rho_{SURF\_EST}}$ suggests that at least some of the 25 pixels in the box around the Villefranche site can be assigned to water. The slope at Villefranche is relatively high pointing to some inaccurate representation of the aerosol model in that region (see Table 5). However, the high correlation and the low RMSE, intercepts, and σ at Villefranche and Venise demonstrate that the chosen approach is very well and consistently applicable over water, too.

[25] There are strong relations between $\overline{\rho_{SURF\_EST}}$ and the performance at the single AERONET sites. Linear regressions of RMSE, bias, and σ as a function of $\overline{\rho_{SURF\_EST}}$ show correlation coefficients of 0.85, 0.84, and 0.88. Also, the nine correlations reported in Table 2 correlate well with the corresponding RMSE (R = −0.82). The largest RMSE, bias, and σ are found at the sites with highest $\overline{\rho_{SURF\_EST}}$, namely at Avignon, Palaiseau, and Toulouse and the lowest values at Villefranche, Venise, ISDGM_CNR, and Ispra. Considering the surface types at the AERONET sites given in Table 1, the sites where water is predominant (Venise and Villefranche) implicate the smallest RMSE. Medium errors are obtained in forest and agriculture areas (Laegeren, Ispra, and Fontainebleau) as well as at ISDGM_CNR. The latter site is located in the City of Venice, an island in the Venetian Lagoon so it is very likely that the corresponding pixel includes a larger part of water. The highest errors occur at Avignon and Toulouse where relatively bright surfaces in man-made environments build the major part of land cover, mainly a combination of (suburban) residential and agriculture areas. As it is commonly known from many studies dealing with the remote sensing of aerosol parameters, ρ_{SURF_EST} is a crucial parameter in the retrieval procedure and the magnitude of the inaccurate estimation usually increases and the aerosol sensitivity decreases with increasing ρ_{SURF}. For instance, *Kaufman and Tanré* [1996] quantified the uncertainty in τ_a to be as high as 0.10 for an error of 0.01 in ρ_{SURF_EST}. The reasons for the underestimation are manifold and are discussed in detail in section 4.2.1.

[26] As the proposed approach considers the anisotropic reflectance characteristics of most natural surfaces (see Figure 2) and the quality of the results (RMSE, bias) seem to depend on ρ_{SURF_EST}, one can expect some diurnal variation of the retrieval accuracy. In addition, discrepancies from the aerosol phase function, ω_0, and particle sphericity as implicit parts of the assumed aerosol model can lead to increased errors [*Chylek et al.*, 2003; *Mishchenko et al.*, 2003], especially at larger scattering angles which occur on account of the fixed observation geometry of geostationary sensors around local noon. To get a better idea of this effect, linear regression analysis is performed in intervals including 75 min (total 81 bins, 9 from each AERONET sites). The number of matchups in the individual bins varies so only bins with a minimum of 30 matchups are considered in the calculations. Figure 4 illustrates the averaged τ_a retrieval error (difference between the SP and SEVIRI matchups) in each of the nine bins as a function of daytime for the three exemplary sites of Avignon, Ispra, and Villefranche. Especially at Avignon a distinct increase around local noon and therefore with lower Sun zenith (or higher scattering angles) can be observed. This effect is much less pronounced and at a lower level for Ispra and not existing at Villefranche. With regard to all sites, a significant correlation of the (binned) τ_a retrieval error and the Sun zenith angle can only be found for Avignon (R = 0.96), Toulouse (R = 0.95), and Ispra (R = 0.91). The AERONET sites of Avignon and Toulouse are situated in suburban areas adjacent to relatively bright agriculture surfaces whose ρ_{SURF_EST} increases significantly during the day. An indirect impact on the diurnal trend of τ_a accuracy might also be attributed to meteorological con-

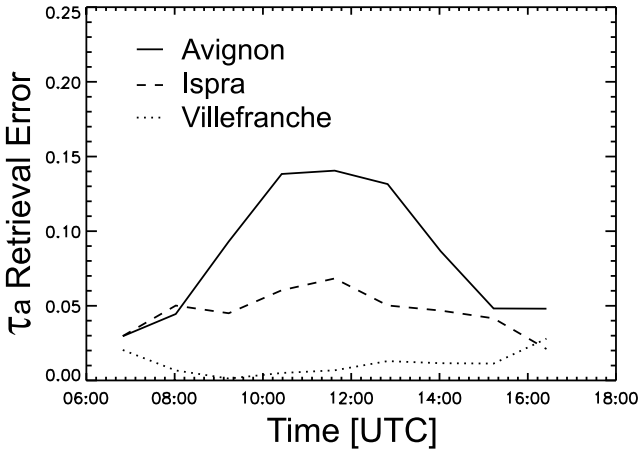

Figure 4. Diurnal trend of the τ_a retrieval error for the Avignon, Ispra, and Villefranche site.

ditions. In particular convection leads to augmented cloud formation in the afternoon during summer and for this reason to increased probability of cloud contamination in retrieved τ_a. Diurnal changes of atmospheric dynamics (e.g., increasing turbulence around noon) probably also cause higher particle concentration and a significant deviation from the initial aerosol model, e.g., through mineral dust emission from dry soils [*Yu et al.*, 2006].

[27] Table 3 summarizes the obtained statistical values analog to Table 2 for the comparison of daily averaged τ_a. The first column shows the number of days for which three or more valid SEVIRI-AERONET pairs could be found to build daily averages. The correlation increases significantly with six sites reaching an R of 0.96 or higher (overall R = 0.94). This clearly illustrates that the 0.6 μm channel of SEVIRI is sensible to an atmospheric aerosol signal even over brighter surfaces, e.g., at the Avignon site despite the high bias. The averaging further reduces the noise in the data set (σ). The RMSE and bias also decrease at almost every site such that at all sites the RMSE is equal to or lower than 0.1.

4.2. Sources of Error

4.2.1. Evaluation of Surface Reflectance Retrieval

[28] The importance of a precise determination of ρ_{SURF_EST} as an indispensable prerequisite for successfully retrieving τ_a has been widely discussed in the literature. An underestimation of ρ_{SURF_EST} generally leads to higher τ_a values and vice versa. The causes of inappropriate image-based ρ_{SURF_EST} retrieval might be manifold, e.g., unclassified cloud shadow pixels, calibration, temporal image coregistration, inaccurate meteorological data, or the a priori made assumptions. Hence ρ_{SURF_EST} shall be evaluated with regard to its accuracy and the assumptions made about the invariability of ρ_{SURF}. Following the ideas of *Hauser et al.* [2005a] and *Knapp et al.* [2005], the basic principle is to atmospherically correct ρ_{TOA} at the AERONET sites taking advantage of the level 2.0 SP measurements (columnar water vapor, τ_a) as well as the 6S radiative transfer code and use the resulting modeled surface reflectance (ρ_{SURF_6S}) as "validation" data. 6S offers the possibility to include the SP inversion products "size distribution" and "refractive index" for the atmospheric correction. Level 1.5 (Version 2) inversion products are used for this purpose because of their high availability (product description and quality criteria can be found at http://aeronet.gsfc.nasa.gov/new_web/optical_properties.html). The advantage of this approach is that it does not require any in situ measurements which would involve different complications to enable an adequate comparison [*Knapp et al.*, 2005]. The major drawback is the different atmospheric path between the SP and SEVIRI and between the SP and the Sun. Even if possible air mass differences are neglected, undetected clouds and subpixel clouds might lead to an overestimation of ρ_{SURF_6S} whereas ρ_{SURF_EST} can be assumed to be cloud and subpixel cloud free. To partly eliminate these random errors, the median of ρ_{SURF_6S} per observation time also is related to ρ_{SURF_EST}.

[29] Figure 5 shows ρ_{SURF_EST} plotted as a function of ρ_{SURF_6S} for all AERONET sites (Figures 5c and 5d) and the ρ_{SURF_EST} and ρ_{SURF_6S} curves for the pixel at Avignon as an example of the evaluation approach (Figures 5a and 5b). Figures 5a and 5c illustrate the initial comparison while Figures 5b and 5d present the comparison based on the calculated median of ρ_{SURF_6S}. The scatter diagrams reveal a clear relationship between the two with a correlation coefficient of 0.93 and 0.97, respectively. In contrary, a majority of the points are below the bisecting line indicating a generally underestimation of ρ_{SURF_EST}. The slopes of the regression lines refer to an overall underestimation of approximately 12% or 7% if the median is used. The linear regression intercepts of zero point to little bias but ρ_{SURF_EST} inaccuracy increases with increasing ρ_{SURF_6S}.

[30] The ρ_{SURF} retrieval errors (the difference between ρ_{SURF_6S} and ρ_{SURF_EST} ($\Delta\rho_{SURF}$)) are diagrammed in Figures 6a and 6c for all AERONET sites and for the exemplary site of Avignon (Figures 6b and 6d). Neither the ρ_{SURF} retrieval errors as a function of daytime nor as a function of the date reveal any apparent trends. On the other

Table 3. Statistical Parameters for the Pixels at the AERONET Sites From Comparing Daily Mean τ_a

AERONET Site	Number of Days	Intercept	Slope	σ	Bias	R	RMSE
All sites	159	0.04	1.01	0.04	0.05	0.94	0.07
Avignon	23	0.08	1.09	0.04	0.09	0.90	0.10
Fontainebleau	9	0.00	1.04	0.02	0.03	0.98	0.04
ISDGM-CNR	24	0.07	0.90	0.03	0.06	0.96	0.06
Ispra	20	0.06	0.91	0.03	0.05	0.97	0.06
Laegeren	11	0.04	1.05	0.03	0.04	0.97	0.05
Palaiseau	8	0.04	1.02	0.04	0.06	0.78	0.07
Toulouse	14	0.03	1.22	0.05	0.07	0.89	0.09
Venise	24	0.01	1.11	0.03	0.04	0.97	0.05
Villefranche	26	−0.02	1.23	0.04	0.03	0.97	0.05

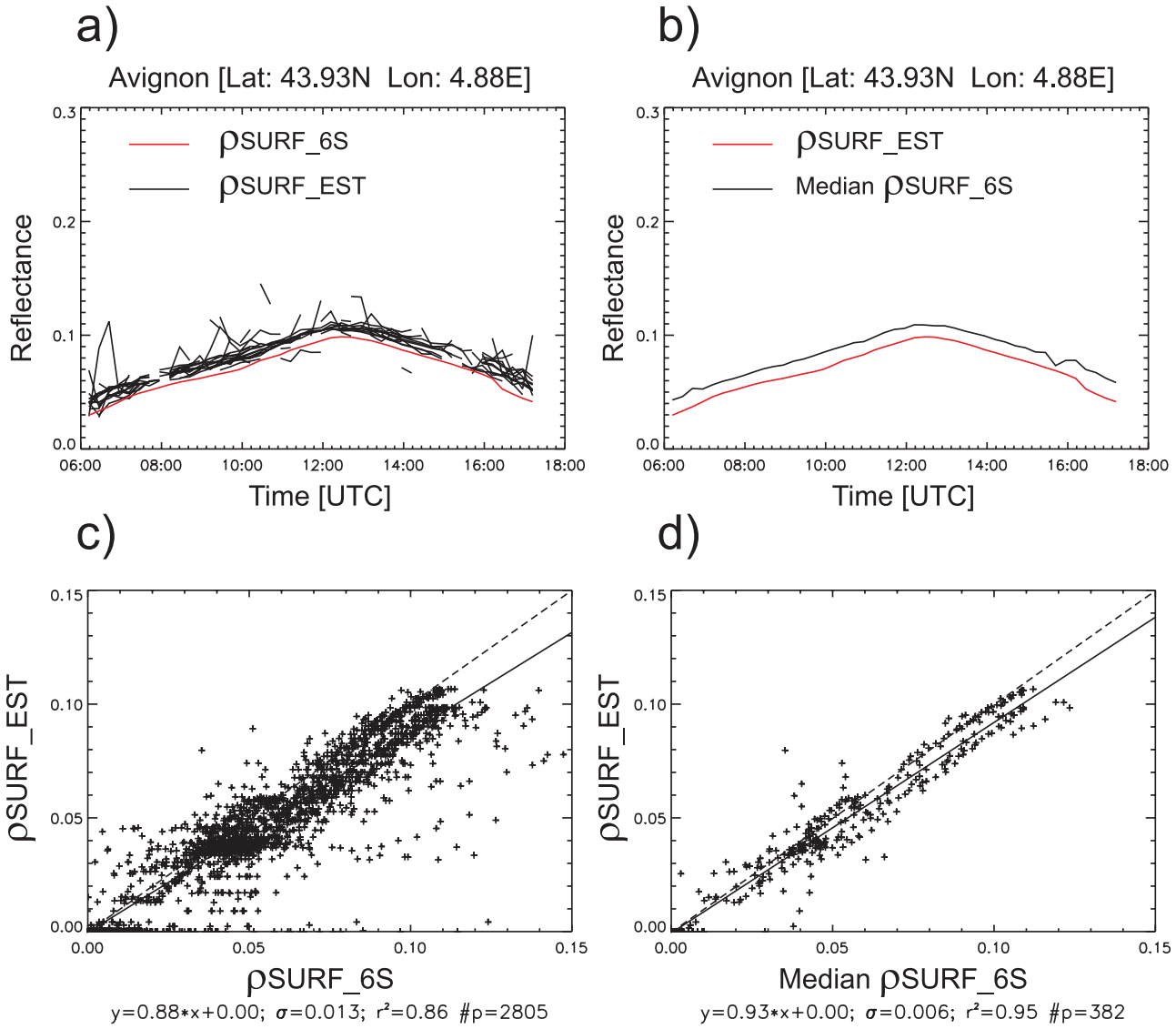

Figure 5. (a and b) Differences between 6S modeled surface reflectance (ρ_{SURF_6S}) and ρ_{SURF_EST} for the pixel at the Avignon AERONET site. (c and d) Scatterplots of ρ_{SURF_EST} as a function of ρ_{SURF_6S} and as a function of the median ρ_{SURF_6S}, including the linear regression line (solid) and the bisecting line (dashed).

hand, $\Delta\rho_{SURF}$ occasionally appears to exhibit some short-term variabilities (Figures 6c and 6d). Such changes might be caused, e.g., by rainfall or drought and bias ρ_{SURF_EST} toward lower values. *Knapp et al.* [2005] stated that ρ_{SURF_EST} tends to decrease with longer time periods mainly because of the increased occurrence of dark observations. Selected statistical parameters from the relation of ρ_{SURF_EST} and the median ρ_{SURF_6S} are summarized in Table 4 for each AERONET site. Apart from Avignon, the $\Delta\rho_{SURF}$ at all sites are well below 0.01 even for brighter surfaces like, e.g., Toulouse. The offset at Avignon can probably be assigned to a strongly absorbing aerosol type found there (see Table 5) such that the assumed continental aerosol type tends to overcorrect ρ_{SURF_EST}. In addition, surface heterogeneity in combination with image coregistration inaccuracies also tends to bias ρ_{SURF_EST} negatively [*Hauser et al.*, 2005a]. The lower $\Delta\rho_{SURF}$ at Venise situated in a very homogeneous area in the Adriatic Sea supports this statement (Table 4). Water introduces different sources of error, i.e., white foams or variable concentrations of suspended matter [*Zhao et al.*, 2003; *Mélin et al.*, 2006]. The reflectance of larger water bodies usually is very small in the wavelength range of SEVIRI's 0.6 μm channel, e.g., the ρ_{SURF_EST} obtained at Venise and Villefranche are in good agreement with *Thieuleux et al.* [2005] who used zero reflectance at 0.6 and 0.8 μm in order to retrieve τ_a and α from SEVIRI over ocean. Applying the described approach allows to get an idea of the accuracy of ρ_{SURF_EST} but because of a lack of available "ground truth" data it is not possible to address the different sources of error in a quantitative manner.

4.2.2. Assumed Background Aerosol Optical Depth

[31] Discrepancies from the assumed background aerosol contamination of $\tau_{a\_bck} = 0.05$ primarily used to precorrect

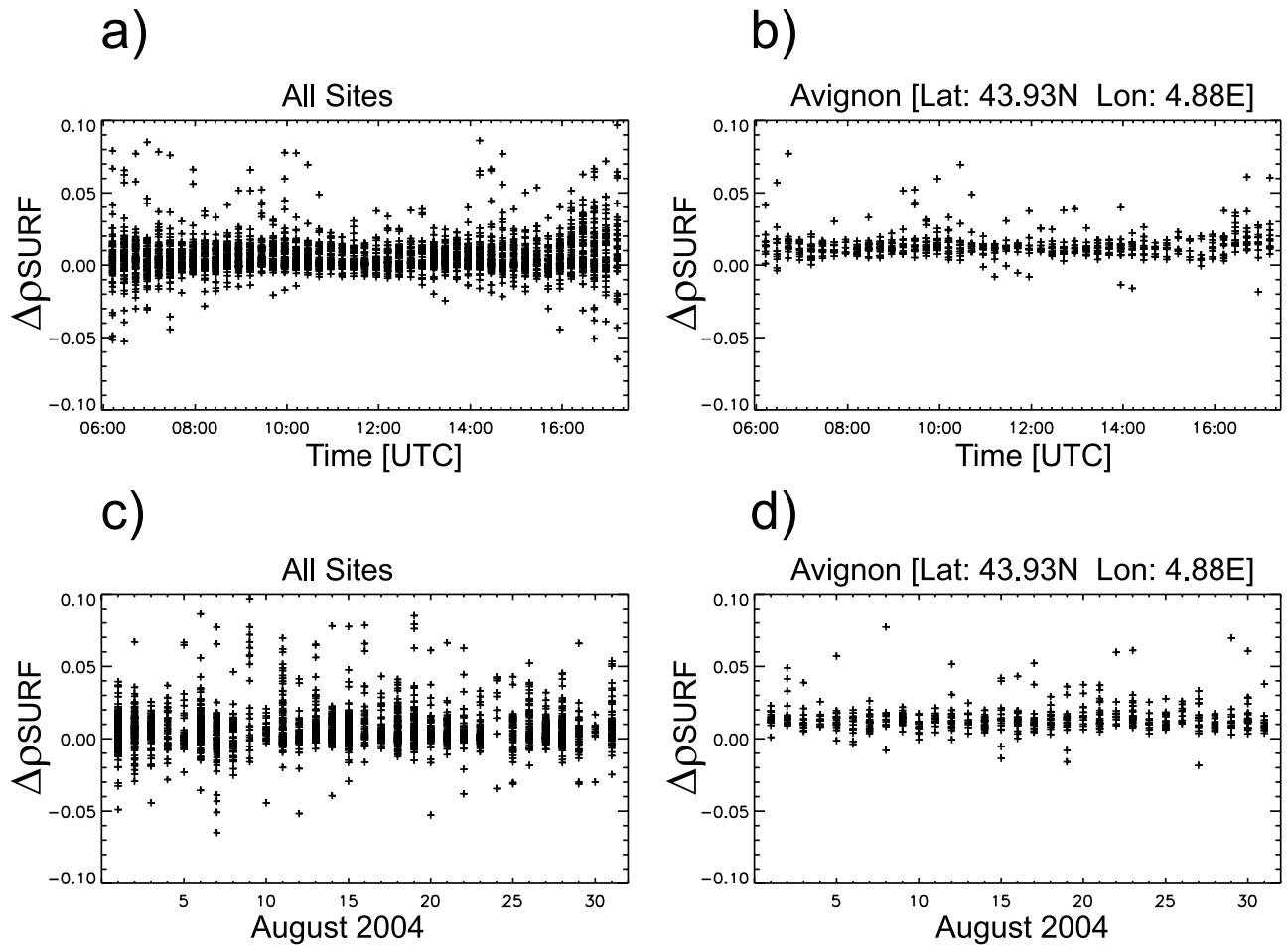

Figure 6. Plots of the ρ_{SURF_EST} retrieval errors ($\Delta\rho_{SURF}$) versus image acquisition (a and b) time and (c and d) date for all pixels at the AERONET sites (Figures 6a and 6c) and for the exemplary site of Avignon (Figures 6b and 6d).

the raw image data set directly influence the results in such a way that an overestimation of τ_{a_bck} finally contributes to an overestimation of retrieved τ_a. The last column of Table 4 shows the average of the lowest 20% SP τ_a at the different sites. An average τ_{a_bck} of 0.049 is found which underlines that the assumption is a good choice considering the entire study area. However, the assumed value underestimates the background aerosol amount in regions with higher cloud coverage, e.g., in the northern part of the study area and overestimates the background aerosol amount in areas with a much smaller cloud coverage, mainly in the southern part. For instance, when discarding the high minimum τ_{a_bck} from the Fontainebleau and Palaiseau sites, the average τ_{a_bck} decreases to 0.040 (±0.012). To test the influence of τ_{a_bck} on the τ_a retrieval accuracy, binned τ_{a_bck} are related to the binned RMSE, bias, and intercept from section 4.1 but no significant relation can be detected. It therefore is concluded that τ_{a_bck} impacts the retrieval much less than other sources of error.

4.2.3. Aerosol Model

[32] The use of a single aerosol model for the European continent is doubtless a strong simplification although the slopes from the linear regression analysis suggested that the continental aerosol model seems appropriate for most parts of the study area. The major continuous exceptions are the occurrence of higher soot concentrations in densely populated or industrialized regions and nondesert mineral dust particles originating from dry soils especially during summer. Table 5 summarizes the monthly averaged ω_0 from the AERONET level 1.5 inversion products and α (between 0.44 and 0.87 μm) from the AERONET level 2.0 climatological table for August 2004. Averaging the 31 daily mean ω_0 from all sites results in a ω_0 of 0.92 (±0.05) and disregarding the low value at Avignon leads to a ω_0 of 0.93 (±0.03) which both are higher than the ω_0 of 0.89 from the assumed continental aerosol model. Plotting the slopes from Table 2 as a function of ω_0 reported in Table 5 does not reveal any correlation. Nevertheless, several studies showed that choosing a more absorbing model can lower the slope or vice versa [e.g., *Zhang et al.*, 2001]. Considering the use of a fixed model, this might improve the retrieval in regions like at Avignon and Toulouse but degrade the performance in other areas, especially if the moderate underestimation of ω_0 through the continental model is taken into account. Computing multiple linear regression of the bias (and RMSE) as a function of ρ_{SURF_EST} (from Table 5) and ω_0 reveals a multiple correlation coefficient of 0.95 (0.94). The partial correlations are 0.81 (0.81) for ρ_{SURF_EST} and −0.83

Table 4. Selected Statistical Parameters From the Evaluation of ρ_{SURF_EST}[a]

AERONET Site	$\overline{\rho_{SURF\_EST}}$	$\overline{Median\rho_{SURF\_6S}}$	$\overline{\Delta\rho_{SURF}}$	$\overline{\tau_{a\_bck}}$
All sites	0.044	0.047	0.003 (±0.007)	0.049 (±0.020)
Avignon	0.070	0.082	0.012 (±0.002)	0.045 (±0.007)
Fontainebleau	0.042	0.037	−0.005 (±0.009)	0.086 (±0.011)
ISDGM-CNR	0.036	0.044	0.008 (±0.008)	0.043 (±0.012)
Ispra	0.025	0.030	0.005 (±0.007)	0.019 (±0.005)
Laegeren	0.048	0.047	−0.001 (±0.003)	0.056 (±0.014)
Palaiseau	0.081	0.085	0.005 (±0.007)	0.072 (±0.007)
Toulouse	0.088	0.089	0.001 (±0.002)	0.048 (±0.007)
Venise	0.000	0.001	0.001 (±0.001)	0.035 (±0.013)
Villefranche	0.000	0.002	0.002 (±0.002)	0.036 (±0.007)

[a]Includes the average of estimated ($\overline{\rho_{SURF\_EST}}$) and modeled ($\overline{Median\rho_{SURF\_6S}}$) surface reflectance and the corresponding mean retrieval error ($\overline{\Delta\rho_{SURF}}$). The last column outlines the average of the 20% lowest τ_a as an approximation of the discrepancy from the assumed background τ_a of 0.05.

(−0.77) for ω_0. Therefore the largest part of the τ_a error can be assigned to this two parameters. Interestingly, a correlation is also found when expressing the slopes as a function of α (R = −0.79). *Abdou et al.* [2005] note that smaller particles usually scatter more light and less τ_a is needed to reach a certain ρ_{TOA}. The Ångström coefficients of continental aerosols are in the range of the values shown in Table 5, e.g., *Hess et al.* [1998] reported a α of 1.45 for an almost identical model named "continental polluted." One has to consider that aerosol type parameters can also vary strongly in space and time, indicated by the standard deviations given in Table 5, e.g., with different synoptic weather situations [*Yu et al.*, 2006]. Additional aerosol regimes might rise from volcanic activity, forest fires, or Saharan dust but there is no evidence that such events occurred during the observed period. Altogether, especially in complex and heterogeneous regions like central Europe it is not possible to select a "perfect" aerosol type and difficult to obtain accurate spatiotemporal aerosol type information matching more or less SEVIRI's resolution.

4.2.4. Other Sources of Error

[33] Inappropriate cloud, subpixel cloud, and cloud shadow masking introduces random and systematic errors [*Zhao et al.*, 2003]. Especially the gradual impact of subpixel clouds is difficult to quantify but impacts the retrieval seriously. The spatial screening in 5 × 5 pixel boxes and the corresponding threshold of 0.05 are able to significantly reduce the impact of cloud related issues. For instance, for a raw processing with no spatial tests applied and simply averaging all τ_a in 5 × 5 pixel boxes, the standard error (from 0.05 to 0.14) and RMSE (0.08 to 0.18) would more than double while the correlation would decrease from 0.9 to 0.6. Calibration inaccuracy is lower than 5% [*Govaerts and Clerici*, 2004]. However, if ρ_{SURF_EST} is derived from the calibrated measurements instead of external sources or information, the effect of calibration inaccuracies tends to reduce since both, ρ_{SURF_EST} and ρ_{TOA} are biased similarly [*Hauser et al.*, 2005a]. Some minor inaccuracies also rise from radiative transfer calculations and the meteorological input data. 6S models surface reflectance with an accuracy of a few percents [*Vermote et al.*, 1997b]. Comparing SMAC to 5S [*Tanré et al.*, 1990] revealed maximum relative errors of less than 5% for different sensors [*Rahman and Dedieu*, 1994] which can be expected to be further minimized after SMAC has been updated to 6S. The largest error due to the sensor-SP-Sun geometry is associated with clouds in the field of view of the satellite sensor. Also, the occurrence of relatively small differences due to SP-SEVIRI time lags, geolocation accuracy, different observed air mass, and higher aerosol loadings in a layer between the SP's height and the ground detected by the remote sensing sensor but not by the SP also seem possible.

4.3. Examples

[34] Different examples shall illustrate the performance of SEVIRI estimated τ_a and its potential use, also in relation to MODIS derived τ_a. Therefore MODIS and SEVIRI τ_a are first compared in a quantitative manner. To get an indication of the MODIS performance during the investigation period and area, Terra and Aqua τ_a are plotted against SP τ_a from the nine sites used herein. The matchup procedure is in accordance to *Ichoku et al.* [2002]. 100 matchups are found and the corresponding scatterplot is illustrated in Figure 7a. The comparison reveals a correlation of 0.84, RMSE of 0.08, bias of 0.05, and a standard deviation of 0.06 which are in the order of the values obtained from the regression analysis of SP τ_a versus SEVIRI τ_a (Table 2). However, the linear regression equation shows some differences to the one calculated for SEVIRI. Whereas SEVIRI tends to overestimate τ_a (intercept = 0.03) MODIS seems to underestimate τ_a at low aerosol concentrations (intercept = −0.03). In contrary, the slope of the regression line is clearly higher (1.26) then the one found for SEVIRI (1.03) pointing to an overestimation of higher τ_a and some deviations from the "true" aerosol type. According to *Levy et*

Table 5. Selected Aerosol Parameters for Addressing the Aerosol Model From AERONET Data[a]

AERONET Site	SSA	Ångström Coefficient
All sites	0.92 (±0.05)	1.48 (±0.21)
Avignon	0.80 (±0.11)	1.38 (±0.30)
Fontainebleau	0.96 (±0.02)	1.31 (±0.40)
ISDGM-CNR	0.92 (±0.05)	1.60 (±0.23)
Ispra	0.92 (±0.05)	1.74 (±0.38)
Laegeren	0.96 (±0.03)	1.58 (±0.34)
Palaiseau	0.90 (±0.05)	1.10 (±0.38)
Toulouse	0.88 (±0.07)	1.61 (±0.50)
Venise	0.96 (±0.03)	1.65 (±0.30)
Villefranche	0.94 (±0.05)	1.32 (±0.32)

[a]The single scattering albedo (level 1.5) is linearly interpolated from 0.44 μm and 0.67 μm to the reference wavelength of 0.55 μm. The Ångström coefficients (from 0.44 to 0.87 μm) in the second column are from the AERONET level 2.0 climatological table.

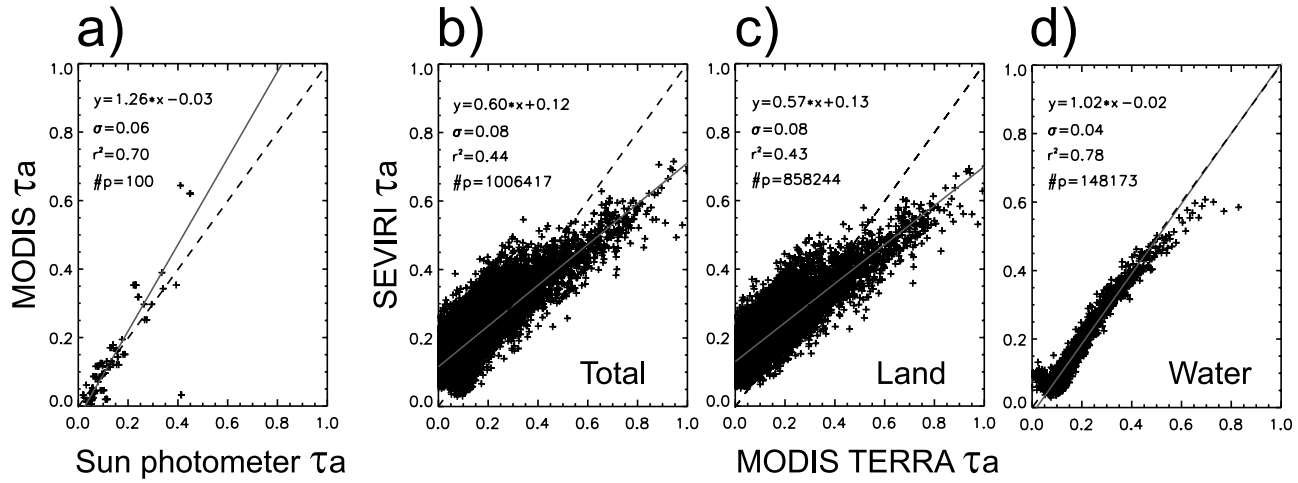

Figure 7. Scatterplots of MODIS versus AERONET Sun photometer and SEVIRI versus MODIS Terra aerosol optical depth with regression line (solid) and bisecting line (dashed).

al. [2007] the MODIS algorithm uses a "nonabsorbing" (urban, industrial) aerosol for the summer months for the central European region with a ω_0 of 0.95. This might partially explain the high slope considering the averaged ω_0 from the different AERONET sites of 0.92. The MODIS algorithm selects the aerosol model as a function of season and location based on AERONET climatology. *Levy et al.* [2007] point out that they decided subjectively on the "nonabsorbing" aerosol model for western Europe as AERONET climatology revealed an even split between the occurrence of "nonabsorbing" and "moderate absorbing" (ω_0 = 0.90) aerosols. *Remer et al.* [2005] reported in their MODIS τ_a validation overestimations of τ_a for western Europe and the Mediterranean region for land in the range of 32% and 48% and for water (Mediterranean Sea) an underestimation of 6%. The values from Figure 7a therefore seem plausible.

[35] Figures 7b and 7c show the scatterplots of SEVIRI τ_a versus MODIS Terra τ_a. Figure 7b includes all matchups, Figure 7c includes only τ_a over land, and Figure 7d includes exclusively those over ocean. Because of the high amount of coincident τ_a, each point shown is an average of 100 binned values sorted after increasing Terra τ_a. The provided statistical parameters are based on the original values. The comparison for the land retrievals combines the negative MODIS intercept from Figure 7 with the positive SEVIRI intercept from Figure 3 to a relatively high offset of 0.13. In addition, the slope of 0.57 points either to an overestimation of MODIS τ_a, an underestimation of SEVIRI, or a combination of both at higher aerosol amounts. The correlation of 0.66 is clearly lower than the one from the linear regression with SP τ_a from both sensors. In contrary to the land comparison, the one over water surfaces is in significant better agreement with a correlation of 0.88, a standard error of 0.04, and an intercept of −0.02. The slope is very close to unity despite the fixed aerosol model used in the SEVIRI processing in contrary to the more sophisticated MODIS approach which estimates the best fit of nine ocean models. The total RMSE is 0.12, the one from the land comparison 0.13, and from the water comparison 0.06. The difference between MODIS and SEVIRI τ_a can be assigned to various reasons. First, at the time of MODIS Terra overpasses (approximately between 0930 and 1200 UTC), the scattering angles can become unfavorable for SEVIRI ($\sim$140° to 160°). This leads to increased SEVIRI retrieval errors mainly in brighter areas with distinctly increased ρ_{SURF_EST} around noon, like demonstrated in section 4.1 for the Avignon and Toulouse AERONET site. Second, the higher spatial resolution of MODIS not only reduces the influence of cloud contamination but also allows to find more suitable pixels for the retrieval. Further, the MODIS algorithm applies a reflectance threshold in the 2.1 μm channel to reject brighter pixels. In this study, with the exception of masked snow covered areas, no such threshold has been applied to obtain a better insight where SEVIRI estimations of τ_a are successful or critical. The MODIS algorithm also takes advantage of different spectral channels and the sensitivity to an aerosol signal is generally higher with shorter wavelength, e.g., in MODIS' 0.43 μm channel compared to SEVIRI's 0.6 μm channel.

4.3.1. Maps of Diurnal Trend

[36] The Po River valley in northern Italy is a highly industrialized and populated region including larger metropolitan areas like Turin, Milano, or Venice as well as dense agriculture activity in between. The three AERONET sites of Ispra, ISDGM_CNR, and Venise are located in or nearby the Po River valley such that this region becomes favorable to demonstrate the capability of SEVIRI to detect diurnal trends of τ_a. Figure 8 shows the evolution of τ_a for the mostly cloud-free day of 1 August 2004 over northern Italy and Figure 9 includes the SP measurements, SEVIRI τ_a, and MODIS retrieval at the three sites mentioned above. A haze event not uncommon in this area [e.g., *Husar et al.*, 2000] occurred in the western part which gradually resolved during the morning. The corresponding decrease of τ_a can be observed at the Ispra site in Figure 9 where the highly congruent AERONET, SEVIRI, and MODIS τ_a are plotted. The upper sequence of eight SEVIRI and one Terra subscene in Figure 8 shows the corresponding τ_a maps in between 0612 UTC and 0942 UTC. The Terra subscene at 0930 UTC exhibits mostly the same spatial pattern as the SEVIRI images but τ_a are slightly higher over the western part compared to the closest two SEVIRI images. Note, that

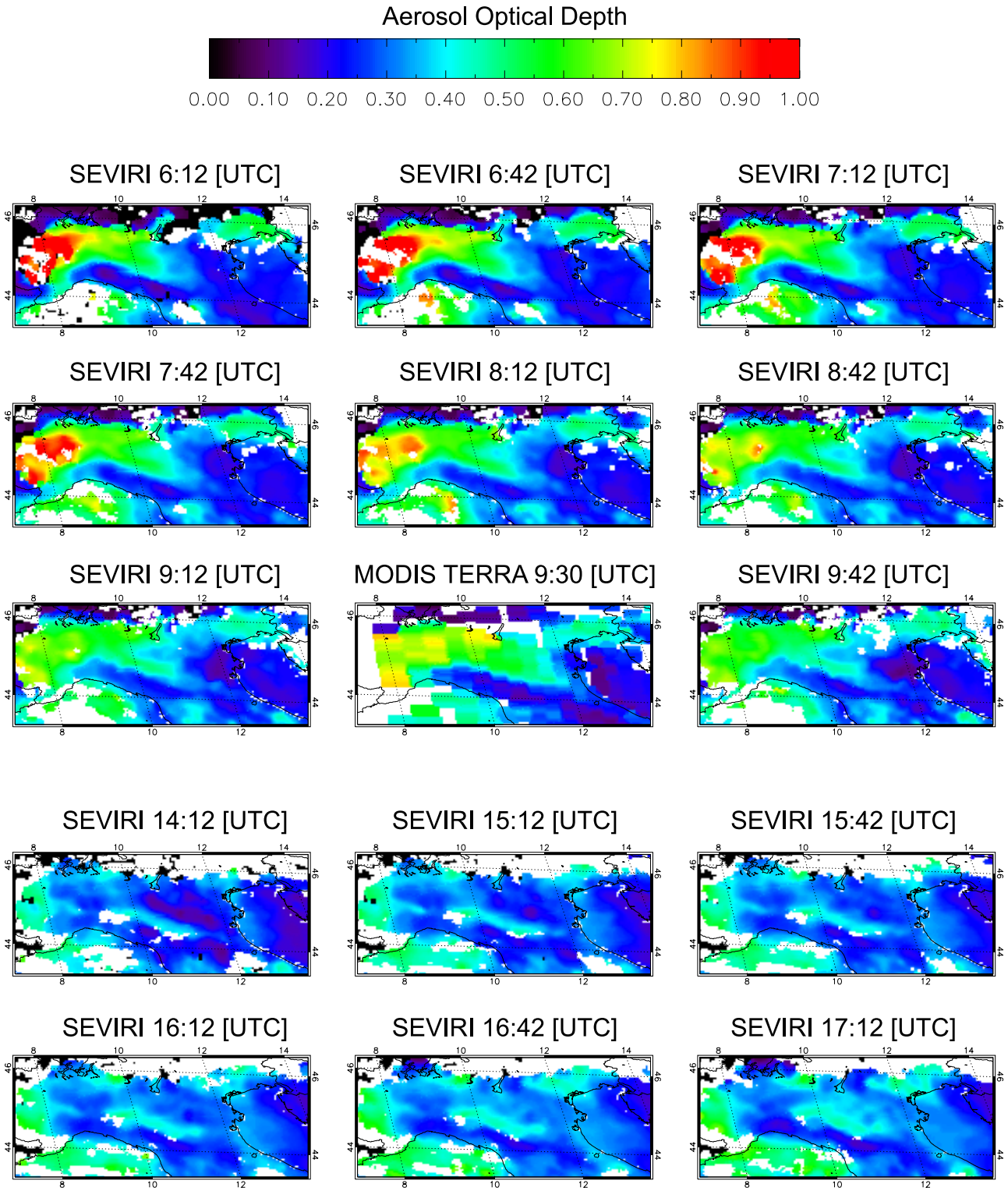

Figure 8. Maps illustrating the evolution of aerosol concentration over northern Italy for 1 August 2004. The maps in the top sequence are from the morning hours, including one MODIS Terra subscene, and the bottom sequence shows the (late) afternoon.

the areas in white are not only cloudy pixels but might also be pixels which failed the tests on spatial consistency (section 3.2). Partially higher τ_a near clouds can be observed around 48°N, 9°E in some subscenes. It remains unclear if this effect is caused by inappropriate cloud masking or the appearance of higher τ_a in the vicinity of clouds. However, it does not seem to be a systematic artifact further indicating that the spatial filtering works well. The transition from land to sea surface can be regarded as a quality indicator in synoptic maps because usually no or

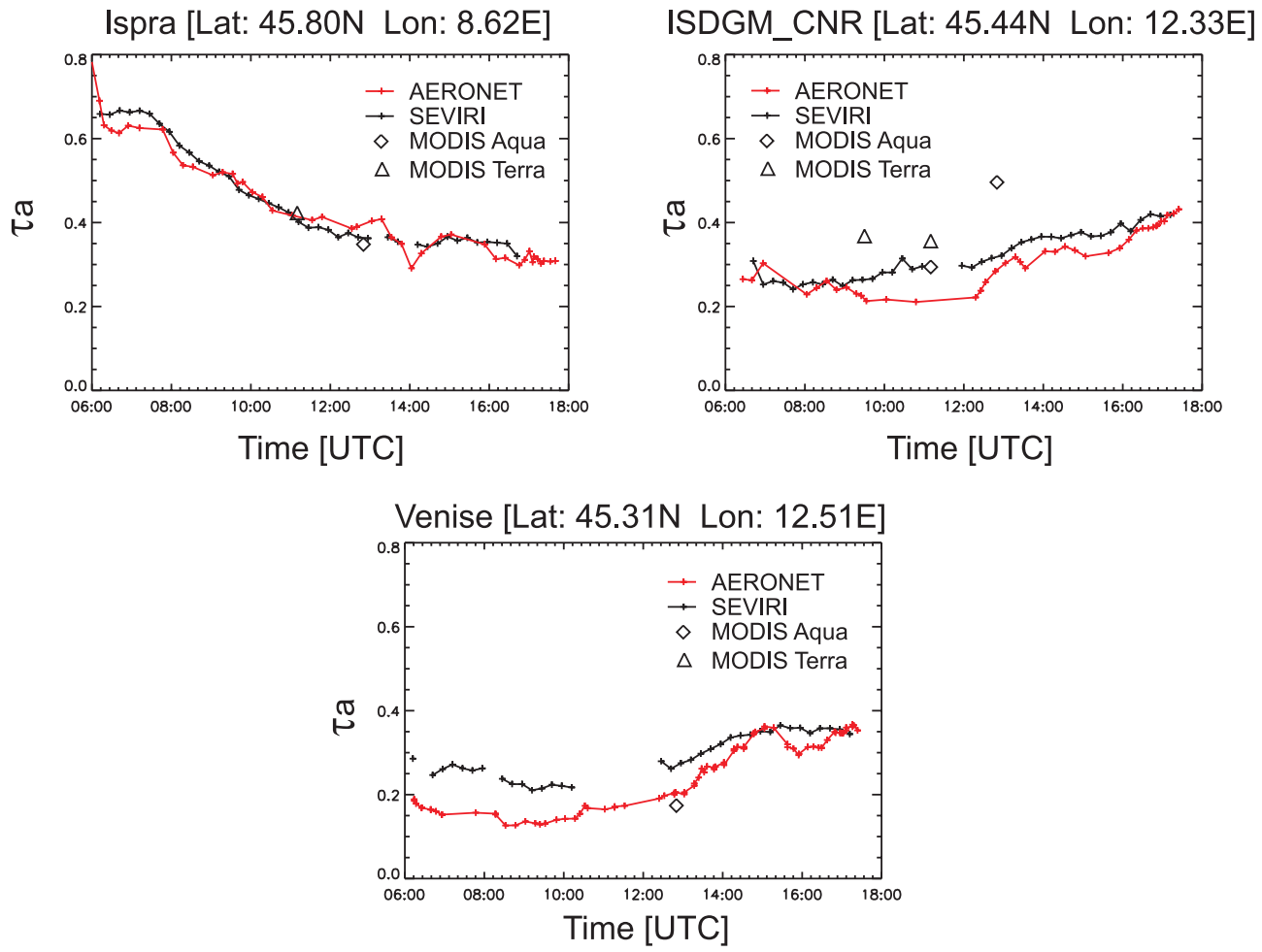

Figure 9. Trend of τ_a for 1 August 2004 at the three northern Italian AERONET sites of Ispra, ISDGM_CNR, and Venise for the SEVIRI results, SP measurements, and MODIS product.

only little contrast of τ_a at the coast is expected. This criterion is mostly fulfilled around the Italian coast as well as for inland water bodies like Lake Garda (~45.5°N, 10.5°E). In contrary to the western part, the diurnal τ_a trend in the eastern part (ISDGM_CNR and Venise, Figure 9) reveals a relatively stable atmospheric aerosol amount in the morning but increasing τ_a in the afternoon. In the lower sequence in Figure 8 ranging from 1412 to 1712 UTC, this increase can clearly be observed over the northern part of the Adriatic Sea where aerosol particles with inland origin are transported eastbound.

[37] The three plots in Figure 9 also illustrate some differences between the SP measurements, MODIS τ_a, and SEVIRI τ_a. At Venise, SEVIRI clearly overestimates τ_a till around 1500 UTC while MODIS Aqua fits the SP value well. The ρ_{SURF_EST} retrieval error from section 4.2.1 for this day shows a decrease from 0.008 in the morning to 0.003 or lower in the afternoon and ω_0 from SP measurements show a decrease from 0.99 to 0.92 during the day. The higher underestimation of ρ_{SURF_EST} and the higher scattering aerosol during the morning explain this offset well. In contrary to Venise, SEVIRI performs better than MODIS at ISDGM_CNR. This site can be considered as a coastal site where subpixel water contamination or surface inhomogeneity likely lead to the observed MODIS offset [*Chu et al.*, 2002].

4.3.2. Monthly Mean Maps

[38] Figure 10 illustrates the monthly averaged τ_a from MODIS (left, Aqua and Terra aggregated) and SEVIRI (right side) based on daily averages. The sample size to calculate monthly mean values is self-explanatory different for the two maps. Similar features occur in both illustrations which correspond well with previous aerosol studies from spaceborne instruments covering the same area and season [*Chu et al.*, 2003; *Hauser et al.*, 2005b]. Decreasing τ_a with higher altitude can clearly be observed, e.g., over the Alps, the Pyrenees, the Vosges mountain range, or the Apennine Mountains in Italy. On the other side, the rugged terrain which leads to shadowing effects and therefore rejected land pixels with ρ_{SURF_EST} less than 0.005 as well as the occurrence of annual snow fields and glaciers in higher parts of the Alps leave some τ_a gaps in the SEVIRI map. The τ_a over sea surfaces are generally low in both maps, but MODIS occasionally shows some enhanced τ_a which might be attributed to a larger impact of single high τ_a events. Both monthly averaged τ_a map reveal some slight "smearing" at the coast, e.g., at the Adriatic coast of Italy, between Corsica and the Italian coast, or to the east of Spain,

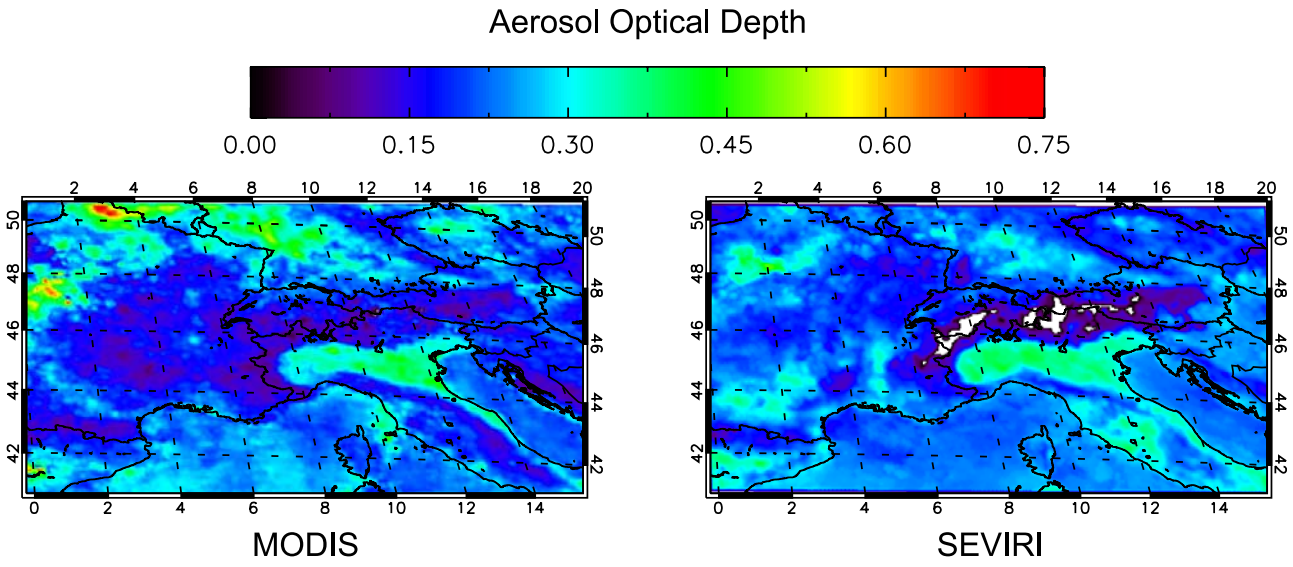

Figure 10. Maps of monthly averaged τ_a for August 2004.

possibly originating from urban or industrial areas along the coastlines [*Mélin et al.*, 2006].

[39] Overall higher aerosol concentrations in both maps can be observed over northern Italy's Po River valley like discussed in section 4.3.1, in Catalonia, Spain (42°N and 0° to 2°E), and in a region around Paris (48°N, 2°E). *Hauser et al.* [2005b] found a similar artifact in northern France in seasonal averaged MODIS τ_a for summer months but not in the corresponding AVHRR derived aerosol maps and AERONET data. They attributed this feature to an imprint of the regional predominant brighter agriculture surface cover in MODIS τ_a. SEVIRI exhibits the same feature but at a lower magnitude and less geographically distributed. On the other side, SEVIRI seems to overestimate τ_a in more southern agriculture areas, like in southern France (44° to 46°N and 5°E) and Tuscany, Italy (43°N, 12°E). These effects are assigned to ρ_{SURF_EST} underestimation and deviations from the continental aerosol model which impact the retrieval accuracy especially at higher scattering angles (e.g., Avignon and Toulouse, section 4.1).

5. Discussion and Conclusion

[40] The objective of this study was to demonstrate the ability of MSG-SEVIRI imagery for the remote sensing of τ_a on a test data set from August 2004 over central Europe. Aerosol optical depth has been estimated by applying a multitemporal approach and it was shown that SEVIRI bears the potential to provide valuable information about atmospheric aerosols. Especially the high temporal resolution not available from polar orbiting sensors enables the tracking of aerosol particles like illustrated in comparison to AERONET SP measurements and the MODIS aerosol product. The results are in good agreement with SP measurements from nine AERONET sites within the study area (R = 0.9, RMSE = 0.08). Compared to MODIS, the results agree very well over water and when considering the different sensor characteristics reasonably over land.

[41] Land surface reflectance is a major limiting parameter when obtaining aerosol information from SEVIRI. The accuracy significantly decreases over bright surfaces even if their surface reflectance can be estimated relatively accurately (like at Toulouse). This leads mainly to two conclusions. Either pixels exceeding a certain threshold are masked out with the consequence of gaps occurring in the diurnal trend or the overestimated τ_a at these pixels are (empirically) corrected after the retrieval. The choice of the aerosol type is another important factor. Regarding the τ_a retrieval over ocean, the studies of *Thieuleux et al.* [2005] and *Brindley and Ignatov* [2006] showed that the inversion of aerosol size parameters (i.e., α) is feasible making use of SEVIRI's 0.6 μm, 0.8 μm, and 1.6 μm channels. Unfortunately, most land surface targets are too bright in the 0.8 μm and 1.6 μm channels and the sensitivity to the aerosol signal becomes too low for an accurate estimation. The observation geometry is an additional factor of limitation. Sun zenith angles before 0612 and after 1712 UTC as well as the satellite viewing angle with higher (or for the Southern Hemisphere lower) latitudes become quite large exceeding the validity range from radiative transfer models like 6S. For this reason, the retrieval for winter months would have to be restricted to less hours. View zenith angles higher than 75° occur around the polar circle for a longitude of 0° decreasing toward lower latitudes with increasing (absolute) longitudes. There is a potential to extend the retrieval of τ_a to other regions and season. In general, the proposed methodology can be applied in areas with moderate to dark surfaces in SEVIRI's 0.6 μm channel, e.g., the tropical rain forests or other vegetated areas in Africa. On the other side, the algorithm is not appropriate for bright areas like snow covered surfaces or deserts like the Sahara. For the latter, algorithms making use of brightness temperature measurements from SEVIRI's six thermal infrared channels (between 3.6 μm and 13.4 μm) are probably able to provide information on dust concentrations [e.g., *Legrand et al.*, 1989; *Wald et al.*, 1998].

[42] The discrepancies found herein point to some necessary refinements of the methodology in advance of a possible operational implementation. For instance, *Hauser et al.* [2005a] related the regional standard deviation to the

retrieval error and used the obtained linear functions to correct retrieved τ_a. This approach bears the potential to compensate for the general underestimation of ρ_{SURF_EST} or regional deviations from the assumed aerosol model. More investigations and validations are needed to determine and improve important parameters used in this study. The ρ_{SURF_EST} underestimation might be reduced choosing a shorter time length with the risk of loosing "aerosol free" observations. This remains an open issue because the optimal time length strongly depends on the location, season, and meteorological conditions. Also, future studies need to address the aerosol model. Primarily over land, SEVIRI's spectral characteristics are not suitable to derive image-based aerosol type information and AERONET inversion products are rather sparsely available in space and time. It therefore seems possible to integrate such information from existing operational aerosol products with good temporal coverage, e.g., α from MODIS [*Remer et al.*, 2005]. The performance of the method will supplementary have to be tested under more comprehensive environmental and meteorological conditions, including, e.g., investigations in different seasons where vegetation changes more rapidly or during wintertime under increased cloud and snow coverage.

[43] *Chylek et al.* [2003] calculated the required accuracy of satellite based τ_a for climate studies (e.g., to address the effect on radiative forcing due to aerosols) to be not more than 0.015 over land and 0.01 over the ocean. Such a precision is apparently not achieved by any of the current operational aerosol products based on satellite measurements. *Kinne et al.* [2003] concluded that satellite data are indeed of essential use for evaluating modeled aerosol characteristics but only if their limitations are considered. In this regard SEVIRI derived τ_a can complement the temporal spacing from polar orbiting instruments. Also, *Wang and Christopher* [2003] found good correlations between τ_a from satellite measurements and particle matter concentrations (PM2.5) usable for estimating air quality categories which might be a future application of SEVIRI τ_a maps. The estimated τ_a of high temporal resolution can therefore, potentially in synergetic use with other aerosol products, provide a great benefit to gain a better understanding of sources, sinks, and atmospheric distribution and dispersion characteristics of aerosols. Such results could then be of interest for society (e.g., monitoring air pollution or visibility) and atmospheric related science, e.g., to study aerosol-cloud interactions.

[44] **Acknowledgments.** The authors would like to thank EUMETSAT and the NASA MODIS team for providing their data products and software. The Swiss Federal Office of Meteorology and Climatology (MeteoSwiss) and the National Center for Environmental Prediction (NCEP) are acknowledged for providing meteorological data. We would also like to thank the AERONET PIs and their staff for establishing and maintaining the sites used in this study. The valuable comments of three anonymous reviewers are highly acknowledged. This study has been funded by the Swiss Defense Procurement Agency.

References

Abdou, W. A., D. J. Diner, J. V. Martonchik, C. J. Bruegge, R. A. Kahn, B. J. Gaitley, K. A. Crean, L. A. Remer, and B. Holben (2005), Comparison of coincident Multiangle Imaging Spectroradiometer and Moderate Resolution Imaging Spectroradiometer aerosol optical depths over land and ocean scenes containing Aerosol Robotic Network sites, *J. Geophys. Res.*, *110*, D10S07, doi:10.1029/2004JD004693.

Ångström, A. (1961), Techniques of determining the turbidity of the atmosphere, *Tellus*, *XIII*, 214–223.

Borde, R., D. Ramon, C. Schmechtig, and R. Santer (2003), Extension of the DDV concept to retrieve aerosol properties over land from the Modular Optoelectronic Scanner (MOS) sensor, *Int. J. Remote Sens.*, *24*(7), 1439–1467.

Brindley, H. E., and A. Ignatov (2006), Retrieval of mineral aerosol optical depth and size information from Meteosat Second Generation SEVIRI solar reflectance bands, *Remote Sens. Environ.*, *102*(3–4), 344–363, doi:10.1016/j.rse.2006.02.024.

Brindley, H. E., and J. E. Russell (2006), Improving GERB scene identification using SEVIRI: Infrared dust detection strategy, *Remote Sens. Environ.*, *104*(4), 426–446, doi:10.1016/j.rse.2006.05.019.

Chu, D. A., Y. J. Kaufman, C. Ichoku, L. A. Remer, D. Tanré, and B. N. Holben (2002), Validation of MODIS aerosol optical depth retrieval over land, *Geophys. Res. Lett.*, *29*(12), 8007, doi:10.1029/2001GL013205.

Chu, D. A., Y. J. Kaufman, G. Zibordi, J. D. Chern, J. Mao, C. Li, and B. N. Holben (2003), Global monitoring of air pollution over land from the Earth Observing System-Terra Moderate Resolution Imaging Spectroradiometer (MODIS), *J. Geophys. Res.*, *108*(D21), 4661, doi:10.1029/2002JD003179.

Chylek, P., B. Henderson, and M. Mishchenko (2003), Aerosol radiative forcing and the accuracy of satellite aerosol optical depth retrieval, *J. Geophys. Res.*, *108*(D24), 4764, doi:10.1029/2003JD004044.

Derrien, M., and H. Le Gléau (2005), MSG-SEVIRI cloud mask and typ from SAFNWC, *Int. J. Remote Sens.*, *26*(21), 4707–4732, doi:10.1080/01431160500166128.

Deuzé, J. L., et al. (2001), Remote sensing of aerosol over land surfaces from POLDER-ADEOS-1 polarized measurements, *J. Geophys. Res.*, *106*(D5), 4913–4926.

Geogdzhayev, I. V., M. I. Mishchenko, E. I. Terez, G. A. Terez, and G. K. Gushchin (2005), Regional advanced very high resolution radiometer-derived climatology of aerosol optical thickness and size, *J. Geophys. Res.*, *110*, D23205, doi:10.1029/2005JD006170.

Govaerts, Y. M., and M. Clerici (2004), MSG-1/SEVIRI Solar Channels Calibration Commissioning Activity Report, *EUMETSAT Tech. Rep. EUM/MSG/TEN/04/0024*, Eur. Organ. for the Exploitation of Meteorol. Satell., Darmstadt, Germany.

Hanson, C., and J. Mueller (2004), Status of the SEVIRI Level 1.5 Data, in *Proceedings of the Second MSG RAO Workshop*, *Eur Space Agency Spec. Publ. ESA SP-582*, 17–21.

Hauser, A., D. Oesch, N. Foppa, and S. Wunderle (2005a), NOAA AVHRR derived aerosol optical depth over land, *J. Geophys. Res.*, *110*, D08204, doi:10.1029/2004JD005439.

Hauser, A., D. Oesch, and N. Foppa (2005b), Aerosol optical depth over land: Comparing AERONET, AVHRR and MODIS, *Geophys. Res. Lett.*, *32*, L17816, doi:10.1029/2005GL023579.

Hess, M., P. Koepke, and I. Schult (1998), Optical properties of aerosols and clouds: The software package OPAC, *Bull. Am. Meteorol. Soc.*, *79*, 831–844.

Holben, B., E. Vermote, Y. J. Kaufman, D. Tanré, and V. Kalb (1992), Aerosol retrieval over land from AVHRR data-application for atmospheric correction, *IEEE Trans. Geosci. Remote Sens.*, *30*(2), 212–222, doi:10.1109/36.134072.

Holben, B. N., et al. (1998), AERONET—A federated instrument network and data archive for aerosol characterization, *Remote Sens. Environ*, *66*, 1–16, doi:10.1016/S0034-4257(98)00031-5.

Husar, R. B., J. D. Husar, and L. Martin (2000), Distribution of continental surface aerosol extinction based on visual range data, *Atmos. Environ.*, *34*, 5067–5078.

Ichoku, C., D. A. Chu, S. Mattoo, Y. J. Kaufman, L. A. Remer, D. Tanré, I. Slutsker, and B. N. Holben (2002), A spatio-temporal approach for global validation and analysis of MODIS aerosol products, *Geophys. Res. Lett.*, *29*(12), 8006, doi:10.1029/2001GL013206.

Ignatov, A., and L. Stowe (2000), Physical basis, premises, and self-consistency checks of aerosol retrievals from TRMM VIRS, *J. Appl. Meteorol.*, *39*(12), 2259–2277.

Ignatov, A., and L. Stowe (2002a), Aerosol retrievals from individual AVHRR channels. Part I: Retrieval algorithm and transition from Dave to 6S radiative transfer model, *J. Atmos. Sci.*, *59*(3), 313–334.

Ignatov, A., and L. Stowe (2002b), Aerosol retrievals from individual AVHRR channels. Part II: Quality control, probability distribution functions, information content, and consistency checks of retrievals, *J. Atmos. Sci.*, *59*(3), 335–362.

Intergovernmental Panel on Climate Change (2001), *Climate Change 2001: The Scientific Basis—Contribution of Working Group I to the Third Assessment of the Intergovernmental Panel on Climate Change*, edited by J. T. Houghton et al., Cambridge Univ. Press, New York.

Jankowiak, I., and D. Tanré (1992), Satellite climatology of Saharan Dust outbreaks: Method and preliminary results, *J. Clim.*, *5*(6), 646–656.

Kaufman, Y. J., and C. Sendra (1988), Algorithm for automatic atmospheric corrections to visible and near-IR satellite imagery, *Int. J. Remote Sens.*, *9*(8), 1357–1381.

Kaufman, Y. J., and D. Tanré (1996), Strategy for direct and indirect methods for correcting the aerosol effect on remote sensing: From AVHRR to EOS-MODIS, *Remote Sens. Environ.*, *55*(1), 65–79.

Kaufman, Y. J., D. Tanré, L. A. Remer, E. F. Vermote, D. Chu, and B. N. Holben (1997a), Operational remote sensing of tropospheric aerosol over the land from EOS-MODIS, *J. Geophys. Res.*, *102*(D14), 17,051–17,061.

Kaufman, Y. J., D. Tanré, H. R. Gordon, T. Nakajima, J. Lenoble, R. Frouin, H. Grassl, B. M. Herman, M. D. King, and P. M. Teillet (1997b), Passive remote sensing of tropospheric aerosol and atmospheric correction for the aerosol effect, *J. Geophys. Res.*, *102*(D14), 16,815–16,830.

King, M. D., Y. J. Kaufman, D. Tanré, and T. Nakajima (1999), Remote sensing of tropospheric aerosols from space: Past, present, and future, *Bull. Am. Meteorol. Soc.*, *80*(11), 2229–2259.

Kinne, S., et al. (2003), Monthly averages of aerosol properties: A global comparison among models, satellite data, and AERONET ground data, *J. Geophys. Res.*, *108*(D20), 4634, doi:10.1029/2001JD001253.

Knapp, K. R. (2002), Quantification of aerosol signal in GOES 8 visible imagery over the United States, *J. Geophys. Res.*, *107*(D20), 4426, doi:10.1029/2001JD002001.

Knapp, K. R., and L. L. Stowe (2002), Evaluating the potential for retrieving aerosol optical depth over land from AVHRR pathfinder atmosphere data, *J. Atmos. Sci.*, *59*(3), 279–293.

Knapp, K. R., T. H. Vonder Haar, and Y. J. Kaufman (2002), Aerosol optical depth retrieval from GOES-8: Uncertainty study and retrieval validation over South America, *J. Geophys. Res.*, *107*(D7), 4055, doi:10.1029/2001JD000505.

Knapp, K. R., R. Frouin, S. Kondragunta, and A. Prados (2005), Toward aerosol optical depth retrievals over land from GOES visible radiances: determining surface reflectance, *Int. J. Remote Sens.*, *26*(18), 4097–4116, doi:10.1080/01431160500099329.

Legrand, M., J. J. Bertrand, M. Desbois, L. Menenger, and Y. Fouquaer (1989), The potential of infrared satellite data for the retrieval of Saharan-Dust optical depth over Africa, *J. Appl. Meteorol.*, *28*, 309–318.

Levy, R. C., L. A. Remer, and O. Dubovik (2007), Global aerosol optical properties and application to Moderate Resolution Imaging Spectroradiometer aerosol retrieval over land, *J. Geophys. Res.*, *112*, D13210, doi:10.1029/2006JD007815.

Liang, S., B. Zhong, and H. Fang (2006), Improved estimation of aerosol optical depth from MODIS imagery over land surfaces, *Remote Sens. Environ.*, *104*(4), 416–425, doi:10.1016/j.rse.2006.05.016.

Martins, J. V., D. Tanré, L. Remer, Y. Kaufman, S. Mattoo, and R. Levy (2002), MODIS Cloud screening for remote sensing of aerosols over oceans using spatial variability, *Geophys. Res. Lett.*, *29*(12), 8009, doi:10.1029/2001GL013252.

Martonchik, J. V., D. J. Diner, R. A. Kahn, T. P. Ackerman, M. E. Verstraete, B. Pinty, and H. R. Gordon (1998), Techniques for the retrieval of aerosol properties over land and ocean using multiangle imaging, *IEEE Trans. Geosci. Remote Sens.*, *36*(4), 1212–1227.

Masuda, K., Y. Mano, H. Ishimoto, M. Tokuno, Y. Yoshizaki, and N. Okawara (2002), Assessment of the nonsphericity of mineral dust from geostationary satellite measurements, *Remote Sens. Environ.*, *82*(2–3), 238–247, doi:10.1016/S0034-4257(02)00040-8.

Mélin, F., M. Clerici, G. Zibordi, and B. Bulgarelli (2006), Aerosol variability in the Adriatic Sea from automated optical field measurements and Sea-viewing Wide Field-of-view Sensor (SeaWiFS), *J. Geophys. Res.*, *111*, D22201, doi:10.1029/2006JD007226.

Mishchenko, M. I., I. V. Geogdzhayev, L. Liu, J. A. Ogren, A. A. Lacis, W. B. Rossow, J. W. Hovenier, H. Volten, and O. Muñoz (2003), Aerosol retrievals from AVHRR radiances: Effects of particle nonsphericity and absorption and an updated long-term global climatology of aerosol properties, *J. Quant. Spectrosc. Radiat. Transfer*, *75–80*, 953–972, doi:10.1016/S0022-4073(02)00331-X.

Moulin, C., F. Guillard, F. Dulac, and C. E. Lambert (1997), Long-term daily monitoring of Saharan dust load over ocean using Meteosat ISCCP-B2 data: 1. Methodology and preliminary results for 1983–1994 in the Mediterranean, *J. Geophys. Res.*, *102*(D14), 16,947–16,958.

Rahman, H., and G. Dedieu (1994), SMAC: A simplified method for the atmospheric correction of satellite measurements in the solar spectrum, *Int. J. Remote Sens.*, *15*(1), 123–143.

Remer, L. A., et al. (2005), The MODIS aerosol algorithm, products, and validation, *J. Atmos. Sci.*, *62*, 947–973.

Schmetz, J., P. Pili, S. Tjemkes, D. Just, J. Kerkmann, S. Rota, and A. Ratier (2002), An introduction to Meteosat Second Generation, *Bull. Am. Meteorol. Soc.*, *83*, 977–992.

Simpson, J. J., and J. R. Stitt (1998), A procedure for the detection and removal of cloud shadow from AVHRR data over land, *IEEE Trans. Geosci. Remote Sens.*, *36*(3), 880–897.

Smirnov, A., B. N. Holben, T. F. Eck, and I. Slutsker (2000), Cloud screening and quality control algorithms for the AERONET data base, *Remote Sens. Environ.*, *73*(3), 337–349, doi:10.1016/S0034-4257(00)00109-7.

Tanré, D., P. Y. Deschamps, C. Devaux, and M. Herman (1988), Estimation of Saharan aerosol optical thickness from blurring effects in thematic mapper data, *J. Geophys. Res.*, *93*(D12), 15,955–15,964.

Tanré, D., C. Deroo, P. Duhaut, M. Herman, J. Morcette, J. Perbos, and P. Y. Deschamps (1990), Description of a computer code to simulate the satellite signal in the solar spectrum: The 5S code, *Int. J. Remote Sens.*, *11*(4), 659–668.

Tanré, D., Y. J. Kaufman, M. Herman, and S. Matteo (1997), Remote sensing of aerosol properties over ocean using the EOS-MODIS spectral radiances, *J. Geophys. Res.*, *102*(D14), 16,971–16,988.

Thieuleux, F., C. Moulin, F. M. Bréon, J. Poitou, and D. Tanré (2005), Remote sensing of aerosols over oceans using MSG/SEVIRI imagery, *Ann. Geophys.*, *23*(12), 3561–3568.

Torres, O., P. K. Barthia, J. R. Herman, A. Sinyuk, P. Ginoux, and B. Holben (2002), A long-term record of aerosol optical depth from TOMS observations and comparisons to AERONET measurements, *J. Atmos. Sci.*, *59*(3), 398–413.

Vermote, E., D. Tanré, J. L. Deuzé, M. Herman, and J.-J. Morcrette (1997a), Second simulation of the satellite signal in the solar spectrum 6S: User guide version 2, Dep. of Geogr., Univ. of Md., College Park.

Vermote, E., D. Tanré, and J.-J. Morcrette (1997b), Second simulation of the satellite signal in the solar spectrum, 6S: An overview, *IEEE Trans. Geosci. Remote Sens.*, *35*(3), 675–686.

Wald, A. E., Y. J. Kaufman, D. Tanré, and B. C. Gao (1998), Daytime and nighttime detection of mineral dust over desert using infrared spectral contrast, *J. Geophys. Res.*, *103*(D24), 32,307–32,313.

Wang, J., and S. A. Christopher (2003), Intercomparison between satellite-derived aerosol optical thickness and PM2.5 mass: Implications for air quality studies, *Geophys. Res. Lett.*, *30*(21), 2095, doi:10.1029/2003GL018174.

Wang, J., S. A. Christopher, F. J. Brechtel, J. Kim, B. Schmid, J. Redemann, P. B. Russell, P. K. Quinn, and B. N. Holben (2003), Geostationary satellite retrievals of aerosol optical thickness during ACE-Asia, *J. Geophys. Res.*, *108*(D23), 8657, doi:10.1029/2003JD003580.

World Meteorological Organization (1983), (CAS)/Radiation Commission of IAMAP Meeting of experts on aerosols and their climatic effects, *WCP 55*, 65 pp., Williamsburg, Va.

Yu, H., et al. (2006), A review of measurement-based assessment of the aerosol direct radiative effect and forcing, *Atmos. Chem. Phys.*, *6*, 613–666.

Zhang, J., S. A. Christopher, and B. N. Holben (2001), Intercomparison of smoke aerosol optical thickness derived from GOES 8 imager and ground-based Sun photometers, *J. Geophys. Res.*, *106*(D7), 7387–7397.

Zhao, T. X.-P., L. L. Stowe, A. Smirnov, D. Crosby, J. Sapper, and C. R. McClain (2002), Development of a global validation package for satellite oceanic aerosol optical thickness retrieval based on AERONET observations and its application to NOAA/NESDIS operational aerosol retrievals, *J. Atmos. Sci.*, *59*(3), 294–312.

Zhao, T. X.-P., I. Laszlo, B. N. Holben, C. Pietras, and K. J. Voss (2003), Validation of two-channel VIRS retrievals of aerosol optical thickness over ocean and quantitative evaluation of the impact from potential sub-pixel cloud contamination and surface wind effect, *J. Geophys. Res.*, *108*(D3), 4106, doi:10.1029/2002JD002346.

Zhao, T. X.-P., O. Dubovik, A. Smirnov, B. N. Holben, J. Sapper, C. Pietras, K. J. Voss, and R. Frouin (2004), Regional evaluation of an advanced very high resolution radiometer (AVHRR) two-channel aerosol retrieval algorithm, *J. Geophys. Res.*, *109*, D02204, doi:10.1029/2003JD003817.

N. Foppa, Swiss Federal Office of Meteorology, CH-8044 Zurich, Switzerland.

A. Hauser, EADS Astrium GmbH, Claude-Dornier-Strasse, D-88090 Immenstaad, Germany.

C. Popp and S. Wunderle, Department of Geography, University of Bern, Hallerstr. 12, CH-3012 Bern, Switzerland. (popp@giub.unibe.ch)